中國機械工程學刊第四十二卷第三期第 263~273 頁(民國一百一十年)
Journal of the Chinese Society of Mechanical Engineers, Vol.42, No.3, pp 263~273 (2021)

Nonlinear and Linear Phenomenon Investigation of Coupled Vibration of a Multi-Disc Rotor Based on Multi-Mistuned Blade Length or Multi-Disordered Straggle Angle Blades

Yi-Jui Chiu *, Ya-Zheng Zhao**, Xiao-Yun Li**, Chia-Hao Yang***, Guo-Fei Yu* and Cheng-Wei Ye**

Keywords： Multi-disk, Assumed mode method, FEM, Coupled vibration, Mistuned and disorder.

ABSTRACT

This study used the finite element method (FEM) and assumed mode method (AMM) to refine the disk-transverse, blade-bending, and shaft-torsion coupling vibration phenomenon of a multi-disc system with multi-mistuned or multi-disordered blades. The authors explore and compare the change regulations of the natural frequencies and mode shapes in the rotor system. Numerical calculation results show that the number of mistuned or disorder blades, as well as their symmetry, will affect the natural frequencies. In a quantitative case, the authors set blade (1) at 10% mistune, and blade (2) has mistune from -10% to +10%. The frequencies of $1a_{11}$ and $1b_{12}$ to $1b_{15}$ modes are unchanged in the length error of blade (2) variation. The frequencies of $1b_{11}$ (SDB) modes decrease from 100.63 Hz to 67.50 Hz, with a blade (2) length error increasing from -10% to 10%. The rotation effect is also explored, and it is found that the mistuned effect becomes complex and unstable.

INTRODUCTION

Paper Received May, 2020. Revised September, 2020. Accepted October, 2020. Author for Correspondence: Yi-Jui Chiu

* *Professor, School of Mechanical and Automotive Engineering, Xiamen University of Technology, Xiamen, 361024, Fujian Province, China.*
***Graduate Student, School of Mechanical and Automotive Engineering, Xiamen University of Technology, Xiamen, 361024, Fujian Province, China.*
**** *Professor,Department of Mechanical Engineering, Taipei Chengshih University of Science and Technology, Taipei, Taiwan*

Rotor vibration has been a problem in the industry and science for more than 100 years. High-speed rotors appeared with the development of industry. They often work in a flexible state, so the problem of vibration and stability is important. Manufacturing errors can cause the center of mass of each segment of a rotor to deviate slightly from the axis of rotation. The resulting centrifugal force will cause transverse vibration during rotation, which is unusually strong at some speeds. Mistuning and disorder problems of rotors are of great concern to scholars.

There has been much research in this field. Gennaro and Leonardo (2004) used artificial neural networks of genetic algorithms to analyze structurally mistuned configurations. They found that leading to the maximum amplitude of the blade vibration with the structural mistuned. Chen and Shen (2015) explored cyclic symmetric rotors with slight mistune. They found that some mode localization phenomena are similar to the authors' work. Li et al. (2014) adopted the finite element method (FEM) to establish models of shaft-disk-blades, blade-disks, and blades. Their results show that some modes are caused by strongly split and coupled vibration. The mistuned cause and affect different coupled vibrations of blades between the disk-blades and the shaft-disk-blades model. Yasharth and Alok (2012) developed a multistage rotor with geometric mistuning via a model. They found two interesting results. First, geometrically mistuned blades can have a reduced-order model. Second, natural frequencies of the two-stage rotor and the statistical distributions of peak maximum amplitudes were produced from Monte Carlo simulations for different patterns of geometric mistuning. Paolo and Giovanni (2012) applied homogenization theory to explore a continuous model of the in-plane vibrations of a mistuned bladed rotor. They also studied localization phenomena and the frequency split arising in the imperfect structure. Alok (2007) formulated an accurate reduced-order model for the development of geometrically mistuned disk-blades. The method was based on the proper orthogonal decomposition of coordinate measuring machine data on blade geometry and the vibration modes of various tuning systems. Hiroki and Akihiro (2012) investigated the effects of a complex pattern on the natural frequencies and frequency response of a mistuned disk-blade system. They found that excitation with the wave number k excites only the vibration modes with the same wave number in the tuned system, and excites all of the vibration modes in the mistuned system. They used sensitivity analysis to achieve the variations of the natural frequencies due to the mistuning pattern. Han (2015) used Floquet theory and the harmonic balance method to analyze isotropic, anisotropic, asymmetric, and general rotors. They found that the modes' corresponding critical speeds are second dominant over the synchronous modes, and the modal line due to weight crosses over the weak modal lines. Lee et al. (2011) utilized a 2-D unsteady vortex lattice method to predict the gust excitation to reach higher engine-order excitation, and determined the forced response characteristics of mistuned bladed disks. Raeisi and Ziaei-Rad (2013) aimed to predict the worst response of a mistuned bladed disk and to develop an integrated method by genetic algorithms and artificial neural networks. They investigated the effect of mistuning on the modulus of elasticity and length of blades on a mistuned blade-disk system. Bai et al. (2014) used hybrid interface substructure component modal synthesis to explore the vibration characteristics of a mistuned blade. They observed that the localization of modal shape is riskier because of mistuned geometric dimensioning. Bai et al. (2015) increased the computational efficiency of a mistuned disk-blade system under the condition of meeting the computational accuracy for a large amount of calculation based on hybrid interface substructure component modal synthesis (IHISCMS). Kwon and Yoo (Kwon et al., 2011, 2015) explored the vibration localization phenomenon of a multi-bundle blade-rotor system. They found that mistuning may cause a significant increase in the forced vibration response of the blade in a multi-package blade system. Critical fatigue problems often occur in mistuned systems, and the forced vibration response of a mistuned system is often significantly larger than that of a tuned system. The above references focus on two subsystems coupled without coupling of the whole multi–disk rotor system.

The authors' previous research adopted an assumed mode method to study a mono-flexible disk system with mistuned blade lengths (2007), a disordered straggle angle blade (2008), and a crack (2008). In 2017, the authors (Zhou et al., 2017; Chiu et al., 2017) used FEM to investigate a multi/single flexible disc-rotor system with springs. The authors used an experimental method to confirm the results of the finite element and assumed mode methods (Chiu et al., 2017; Yu et al., 2019).

The current research investigates the coupled phenomenon among blade-bending, disk-bending, and shaft-torsion. Based on our previous research (Chiu et al., 2007; Chiu et al., 2008; Chiu et al., 2008; Zhou et al., 2017; Chiu et al., 2017; Chiu et al., 2017; Yu et al., 2019), we focused on coupled vibration of a multi-disc system based on mistuned blades length or disordered straggle angle. The blades are considered an Eular type with stagger angle, and the discs are supposed to be flexible in this turbine rotor system. We employed ANSYS engineering software and FEM to analyze it. We discuss the rotor change regulations of mode shapes and natural frequencies. This research aims to provide a qualitative and quantitative overview for the multi-flexible disc system.

THEORETICAL ANALYSIS

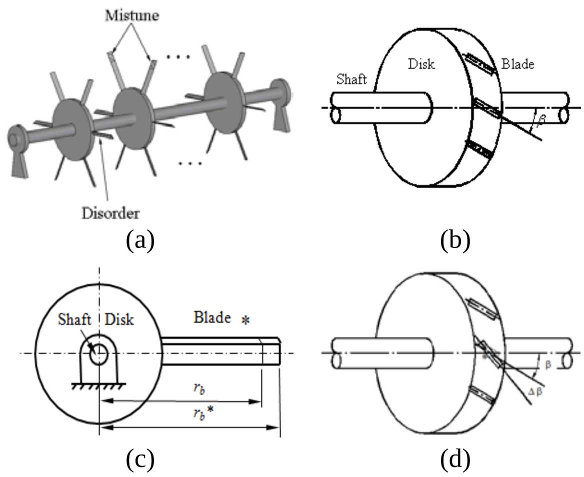

Fig.1. (a) A general multi-disc rotor with mistuned and disordered blade; (b) straggle angle; (c) length mistuned blade; and (d) angle disorder blade.

A general rotor system with mistuned and disorder blades is shown in Figure 1. The rotor includes four subsystems, such as shaft, multi-flexible disc, blades and the blades with length mistuned blade and disorder. The blades have a straggle angle. The mistuned-length blades are marked with an asterisk, and the coordinates are given as follows:

$$r_b^* = r_b + \Delta r = r_b(1+\varepsilon_l), \quad (1)$$

Where ε_l is the mistuned blade deviation ratio, negative or positive.

The blade of disorder stagger angle is indicated by an asterisk, and is written as follows:

$$\beta^* = \beta + \Delta\beta = \beta(1+\varepsilon_a), \quad (2)$$

where ε_a is the disorder error, positive or negative.

The shaft-disk subsystem torsion energy equations are as follows (Chiu et al., 2007):

$$T_s = \frac{1}{2}\int_0^{Ls} I_s(\dot{\phi}+\Omega)^2 dZ + \frac{I_d}{2}(\dot{\phi}+\Omega)^2|_{Z=Z_d}, \tag{3}$$

$$U_s = \frac{1}{2}\int_0^{Ls} G_s J_s\left(\frac{\partial \phi}{\partial Z}\right)^2 dZ, \tag{4}$$

where $\phi(Z,t)$ is the displacement of torsion in a rotating frame; the shaft length, inertia polar moment, and torsion rigidity are respectively L_s, I_s and $G_s J_s$; and the polar moment of inertia of the disk is I_d .The upper dot indicates the time derivative, and subscripts d and s indicate disk and shaft, respectively.

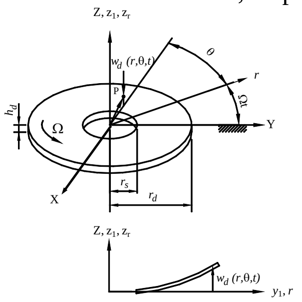

Fig 2. Coordinates and geometry of rotating disk

Figure 2 shows a disk, free outside and fixed inside, rotating at a constant speed Ω. The outer and inner radius of the disk are r_d and r_s, respectively, and h_d is the disk's thickness.

The disk's transverse vibration energy equations are as follows (Chiu et al., 2007):

$$T_d = \frac{\rho_d h_d}{2}\int_{r_s}^{r_d}\int_0^{2\pi}\left(\dot{w}_d + \Omega\frac{\partial w_d}{\partial \theta}\right)^2 r d\theta dr, \tag{5}$$

$$U_d = \frac{D}{2}\int_{r_s}^{r_d}\int_0^{2\pi}\left\{(\nabla^2 w_d)^2 - (1-\nu)\frac{\partial^2 w_d}{\partial r^2}\left[\left(\frac{1}{r}\frac{\partial w_d}{\partial r}+\frac{1}{r^2}\frac{\partial^2 w_d}{\partial \theta}\right) - \left(\frac{1}{r}\frac{\partial^2 w_d}{\partial r \partial \theta}-\frac{1}{r^2}\frac{\partial w_d}{\partial \theta}\right)^2\right]\right\} r d\theta dr$$
$$+\frac{h_d}{2}\int_{r_s}^{r_d}\int_0^{2\pi}\left[\sigma_r\left(\frac{\partial w_d}{\partial r}\right)^2 + \sigma_\theta\left(\frac{1}{r}\frac{\partial w_d}{\partial \theta}\right)^2\right] r d\theta dr, \tag{6}$$

The disk's transverse displacement uses w_d. The bending rigidity uses D. ∇^2 is the Laplacian; the initial radial stresses due to Ω use σ_r, and the circumferential directions use σ_θ.

The following are the terms:

$$\nabla^2 = \frac{\partial^2}{\partial r^2} + \frac{\partial}{r\partial r} + \frac{\partial^2}{r^2 \partial \theta^2}, \tag{7}$$

$$D = \frac{E_d h_d^3}{12(1-\nu^2)}, \tag{8}$$

$$\sigma_r = \frac{3+\nu}{8}\rho_d \Omega^2 (r_d^2 - r^2)$$
$$+\frac{(1-\nu)\rho_d \Omega^2 r_s^2[(3+\nu)r_d^2-(1+\nu)r_s^2]}{8[(1+\nu)r_d^2+(1-\nu)r_s^2]}\left(\frac{r_d^2}{r^2}-1\right), \tag{9}$$

$$\sigma_\theta = \frac{\Omega^2}{8}[(3+\nu)r_d^2-(1+3\nu)r^2]$$
$$-\frac{(1-\nu)\rho_d \Omega^2 r_s^2[(3+\nu)r_d^2-(1+\nu)r_s^2]}{8[(1+\nu)r_d^2+(1-\nu)r_s^2]}\left(\frac{r_d^2}{r^2}+1\right). \tag{10}$$

Figure 3 shows a rotating cantilevered blade on a flexible disk with stagger angle β. The *(X,Y,Z)* coordinate system is the inertia frame, and the (x_1,y_1,z_1) frame rotates at a constant speed Ω. The (x_2,y_2,z_2) frame rotates at straggle angle β relative to the (x_1,y_1,z_1) frame, and the (x_3,y_3,z_3) frame is clamped to the root of the blade.

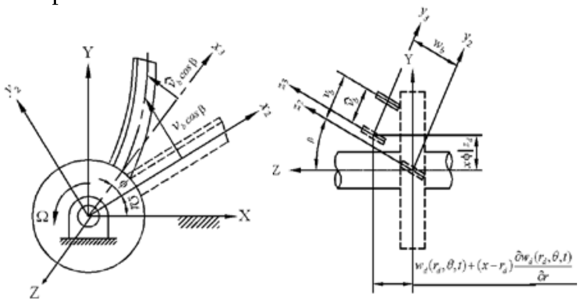

Fig 3. Blade deformation and coordinate builds.

The blade's kinetic and strain energies equations are as follows (Chiu et al., 2007):

$$T_b = \frac{1}{2}\int_{r_d}^{r_b}\rho_b A_b\left\{\begin{matrix}\dot{v}_b^2+\dot{w}_b^2+(v_b\cos\beta+w_b\cos\beta)^2\Omega^2\\ +x^2\Omega^2+2x(\dot{v}_b\sin\beta+\dot{w}_b\sin\beta)\Omega\end{matrix}\right\}dx$$
$$+\frac{1}{2}\int_{r_d}^{r_b} I_b\left(\Omega\cos\beta+\frac{\partial \dot{v}_b}{\partial x}\right)^2 dx, \tag{11}$$

$$U_b = \int_{r_d}^{r_b}\frac{E_b I_A}{2}\left(\frac{\partial^2 v_b}{\partial x^2}\right)^2 dx$$
$$+\int_{r_d}^{r_b}\frac{1}{4}\Omega^2\rho_b A_b(r_b^2-x^2)\left[\left(\frac{\partial v_b}{\partial x}\right)^2+\left(\frac{\partial w_b}{\partial x}\right)^2\right]dx, \tag{12}$$

The y_2 and z_2 directions of transverse displacements use v_b and w_b. I_A is the area moment of inertia about the z_3 axis, and I_b is the polar moment of inertia.

The total blade displacements $v_b(x,t)$ and $w_b(x,t)$ are the shaft's torsion displacement $\phi(Z_d,t)$; the transverse displacement of the disk uses w_d and the bending blade displacement $\hat{v}_b(x,t)$. The kinematic relations between these displacements are as follows:

$$v_b(x,t) = \hat{v}_b + x\phi|_{Z_d}\cos\beta - (w_d|_{r_d} + xw_d'|_{r_d})\sin\beta, \tag{13}$$

$$w_b(x,t) = x\phi|_{Z_d}\sin\beta + (w_d|_{r_d} + xw_d'|_{r_d})\cos\beta. \tag{14}$$

The assumed mode method (AMM) is used to discretize the continuous system:

$$\phi(Z,t) = \sum_{i=1}^{n_s}\Phi_i(Z)\eta_i(t) = \Phi(Z)\eta(t), \tag{15}$$

$$w_d(r,\theta,t) = \sum_{i=1}^{n_d}[W_i^c(r,\theta)\zeta_i^c(t) + W_i^s(r,\theta)\zeta_i^s(t)]$$
$$= W(r,\theta)\zeta(t), \tag{16}$$

$$\hat{v}_{b_k}(x,t) = \sum_{i=1}^{n_b}V_i(x)\xi_{ik}(t) = V(x)\zeta_k(t), \tag{17}$$

The mode shapes of the bending blade, transverse disk, and torsion shaft use $V_i, \{W_i^c, W_i^s\}, \Phi_i$.

$\eta_i, \zeta_i^c, \zeta_i^s, \xi_{ik}$ are the participation factors. n_s,n_d,n_b are subscripts of the corresponding sub-units, are the modes number seemed suit for permissible accuracy. (n_b,n_d,n_s)=(11,10,8) is good for yield accuracy up to 10^{-5} Hz in this paper. These modes are as follows:

$$\Phi_i(Z) = \sin[\frac{(2i-1)\pi Z}{2L_s}], \tag{18}$$

$$W_i^c(r,\theta) = R_i(r)\cos[(i-1)\theta], \tag{19}$$

$$W_i^s(r,\theta) = R_i(r)\sin[(i-1)\theta], \tag{20}$$

where $R_i(r)$ is the radial function of the disk and choose the beam function.

$$V_i(x) = (\sin\tau_i x - \sinh\tau_i x) + \alpha_i(\cos\tau_i x - \cosh\tau_i x), \tag{21}$$

is a beam function for a blade with

$$[\cos\tau_i(r_b - r_d)][\cosh\tau_i(r_b - r_d)] + 1 = 0, \tag{22}$$

$$\alpha_i = \frac{-\sin\tau_i(r_b - r_d) - \sinh\tau_i(r_b - r_d)}{\cos\tau_i(r_b - r_d) + \cosh\tau_i(r_b - r_d)}, \tag{23}$$

The above equations alter the Lagrange equations yields employment and the energy expression. The discretizated equations of motion in matrix notation are as follows:

$$[M]\ddot{q} - \Omega[P]\dot{q} + ([K^e] + [K^i] - \Omega^2[K^\Omega])q = 0, \tag{24}$$

$-\Omega[P]$ induces natural frequency bifurcation, obtained from the Coriolis effect. Note, if the disk is flexible and [P] is not zero. So, the disk is flexible and the frequency could be bifurcating. $[K^e]$ is observed from the elastic deflection at low rotational speed. $[K^i]$ is the stiffness form rotation with initial stress. $-\Omega^2[K^\Omega]$, observed from the rotor rotation, softening it becomes very obvious at high speed. That is significant to the rotor stability effect. The matrices $[M],[P],[K^e],[K^i],[K^\Omega]$ are displayed in the appendix. The above matrices have dimension $(n_s + 2N_d \times n_d + N_d \times N_b \times n_b) \times (n_s + 2N_d \times n_d + N_d \times N_b \times n_b)$, and N_b and N_d are the numbers of blades and disks, respectively. The items of the above matrices are shown in the appendix. q is a generalized vector:

$$q = \{\eta^T \setminus \zeta^{cT}\zeta^{sT} \setminus \xi_1^T\xi_2^T \cdots \xi_N^T\}^T, \tag{25}$$

Free vibration analysis in an ordinary way, that is a hypothetical solution which is of the form $q = \{c\}e^{\lambda t}$ with $\{c\}$ the undetermined coefficient vector and λ is the eigenvalue.

FINITE ELEMENT METHODS

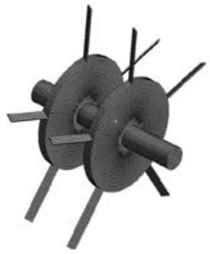

Fig 4. Gerneral FE mesh of multi-disc rotor

Three kinds of FEM software were used to simulate a rotor system (Chiu et al., 2017; Chiu et al., 2017). Based on the results, we found ANSYS best, with errors less than 1%, and we use FEM and ANSYS to calculate the shaft-disk-blade system in this paper. Table 1 shows the material and geometric parameters used in AMM and FEM. Figure 4 is a general FE mesh. The element types of the subsystem in the rotor system were simulated many times to obtain results for different frequencies. The perfect element types are that the blades, disks and shaft are chose 3D hexahedral solid elements. The single-disk rotor system used 70,000 nodes and 60,000 elements, and the two-disk rotor system used 110,000 nodes and 100,000 elements. The shaft torsion vibration boundary condition is clamped-free.

Table 1. Geometric and material properties

Shaft	density: ρ_s	7850 kg/m^3
	shear modulus: G_s	75 Gpa
	shaft length: L_s	0.6 m
	radius: r_s	0.04 m
Disk	density: ρ_d	7850 kg/m^3
	Young's modulus: E_d	200 Gpa
	location: z_d	0.3 m
	outer radius: r_d	0.2 m
	thickness: h_d	0.03 m
	Poisson's ratio: ν	0.3
Blade	density: ρ_b	7850 kg/m^3
	Young's modulus: E_b	200 Gpa
	blade outer end: r_b	0.4 m
	cross-section: A_b	1.2×10^{-4} m^2
	area moment of inertia: I_A	1.92×10^{-9} m^2
	Straggle angle: β	30°

NUMERICAL RESULTS

Table 2 lists the natural frequencies (NFs) of subunits on coupled vibration. These are used as numerical results for interpretation and verification.

Table 2. NF (Hz) of subunits

Component's NF	ω_1	ω_2	ω_3
shaft-disk (w/o blades)	207.418	2645.690	5267.204
disk (shaft rigid)	921.227	974.922	1205.039
clamped blade (shaft-disk rigid)	81.538	510.99	1430.788

Its range is from the root of the blade (0) to its tip (1). Figures 5–16 and Tables 2–6 bewrote at no rotation (Ω=0). The reasons are that the shaft torsion vibration boundary condition is clamped free. If the boundary is different, then the selected modes could be transformed. The modes of a rotating rotor system are called the traveling modes of its non-rotating modes.

Table 3. Six modes of NF (Hz) of five blades and single flexible disk with mistuned blades (±10%) using two methods

Mode	AMM (Tune)	FEM (Tune)	Deviation (%)	AMM (+10%) (mistune,1)	FEM (+10%) (mistune,1)	Deviation (%)
$1a_{11}$	80.891 (SDB)	81.020 (SDB)	0.159	67.254 (SDB)	67.411 (SDB)	0.233
$1b_{11}$	81.422 (DB)	81.615 (DB)	0.237	81.285 (SDB)	81.199 (SDB)	-0.106
$1b_{12}$	81.492 (DB)	81.631 (DB)	0.171	81.47 (SDB)	81.666 (SDB)	0.241
$1b_{13}$	81.538 (BB)	81.670 (BB)	0.161	81.538 (BB)	81.702 (BB)	0.201
$1b_{13}$	81.538 (BB)	81.671 (BB)	0.163	81.538 (BB)	81.706 (BB)	0.206
$1c_{11}$	202.777 (SDB)	203.250 (SDB)	0.237	202.777 (SDB)	202.95 (SDB)	0.085
Mode	AMM (-10%) (mistune,1)	FEM (-10%) (mistune,1)	Deviation (%)	AMM (+10%) (mistune,1,2)	FEM (+10%) (mistune,1,2)	Deviation (%)
$1a_{11}$	100.35 (SDB)	100.33 (SDB)	-0.020	67.254 (SDB)	67.327 (SDB)	0.109
$1b_{11}$	81.284 (SDB)	81.034 (SDB)	-0.308	67.254 (SDB)	67.495 (SDB)	0.358
$1b_{12}$	81.47 (SDB)	81.478 (SDB)	0.010	81.285 (SDB)	81.327 (SDB)	0.052
$1b_{13}$	81.538 (BB)	81.544 (SDB)	0.007	81.47 (SDB)	81.7 (SDB)	0.282
$1b_{13}$	81.538 (BB)	81.618 (SDB)	0.098	81.538 (BB)	81.701 (BB)	0.200
$1c_{11}$	202.777 (SDB)	203.68 (SDB)	0.445	202.777 (SDB)	202.58 (SDB)	-0.097

This study is based on the research (Chiu et al., 2007; Chiu et al., 2008), whose results we expand by researching the more complex phenomena in a multi-disk system. And in order to make the phenomenon obviously appear, this study adopts larger error. For example, mistuned blades length adopted ±10% and disordered straggle angle adopted +30°. Tables 3 and 4 show the six/seven modes of natural frequencies of a five-/six-blade and single flexible disk system with mistuned blades by two methods. Fig.5 shows how the frequency varies with a five- or six-blade system with mistuned blades in the rotor.

Table 4. Seven modes of NF (Hz) of six-blades and single flexible disk system with mistuned blades (±10%) using two method.

Mode	AMM (Tune)	FEM (Tune)	Deviation (%)	AMM (+10%) (mistune,1)	FEM (+10%) (mistune,1)	Deviation (%)
$1a_{11}$	80.770 (SDB)	81.380 (SDB)	0.755	67.342 (SDB)	67.418 (SDB)	0.113
$1b_{11}$	81.423 (DB)	81.572 (DB)	0.183	81.217 (SDB)	81.058 (SDB)	-0.196
$1b_{12}$	81.438 (DB)	81.575 (DB)	0.168	81.255 (SDB)	81.658 (SDB)	0.496
$1b_{13}$	81.496 (DB)	81.634 (DB)	0.169	81.441 (SDB)	81.671 (SDB)	0.391
$1b_{14}$	81.538 (BB)	81.668 (BB)	0.159	81.538 (BB)	81.687 (BB)	0.183
$1b_{14}$	81.538 (BB)	81.669 (BB)	0.161	81.538 (BB)	81.689 (BB)	0.185
$1c_{11}$	201.921 (SDB)	203.540 (SDB)	0.802	201.822 (SDB)	201.64 (SDB)	-0.09
Mode	AMM (-10%) (mistune,1)	FEM (-10%) (mistune,1)	Deviation (%)	AMM (+10%) (mistune,1,2)	FEM (+10%) (mistune,1,2)	Deviation (%)
$1a_{11}$	99.97 (SDB)	100.36 (SDB)	0.39	67.296 (SDB)	67.331 (SDB)	0.052
$1b_{11}$	81.208 (SDB)	81.171 (SDB)	-0.046	67.349 (SDB)	67.506 (SDB)	0.233
$1b_{12}$	81.267 (SDB)	81.664 (SDB)	0.489	81.219 (SDB)	81.179 (SDB)	-0.049
$1b_{13}$	81.357 (SDB)	81.671 (SDB)	0.386	81.413 (SDB)	81.662 (SDB)	0.306
$1b_{14}$	81.538 (BB)	81.681 (BB)	0.175	81.538 (BB)	81.679 (BB)	0.173
$1b_{14}$	81.538 (BB)	81.694 (BB)	0.191	81.538 (BB)	81.693 (BB)	0.190
$1c_{11}$	202.505 (SDB)	202.24 (SDB)	-0.131	201.559 (SDB)	201.99 (SDB)	0.214

For a five-blade and single flexible disk system (Chiu et al., 2007), the coupling modes can be displayed in three groups: SDB, DB, and BB. The BB repeated modes were of $N_b/2$ and $(N_b-1)/2$ for even and odd numbers of blades. The $1a_{11}$ to $1b_{13}$ modes belong to one group led by the blade's first mode. $1c_{11}$ mode is led by the shaft's first mode. These mistuned blades locate in asymmetric places. 1a–1b modes are groups in which the blade's first mode predominates in a five-blade system. Note that the modes change phenomena, and that this Fig.5 is not drawn to a linear scale. It has two reference marks, ω = 81.538 and 207.43, which indicate that the system frequencies predominate by cantilevered first bending of the blade and first torsion of the shaft (Table 2).

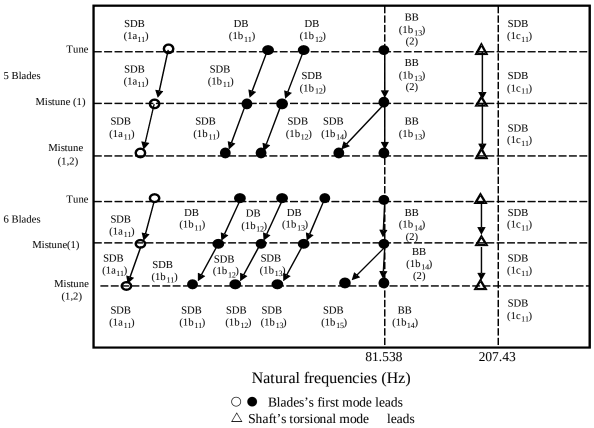

Fig. 5. Frequency variation based on asymmetric mistuned blade in a six-/five-blade and single-disk system.

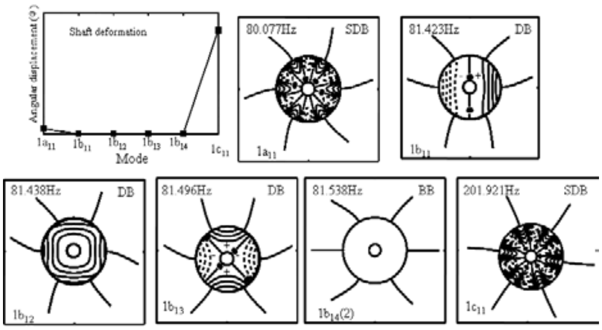

Fig. 6. Seven modes of a six-blade and single-disk rotor using AMM.

Three phenomena are found in Fig.5 and Tables 3 and 4. First, when a mistune appears in a blade, the shaft-disk-blade system only has two types of coupled modes, which are SDB and BB. Disk-blade (DB) modes vanish because the mistune destroys the system symmetry and the balance between disks and blades no longer exists. The second is that two mistune blades appear in two asymmetric blades, the frequencies of $1a_{11}$, $1b_{11}$ and $1b_{12}$ modes drop again. The repeat frequencies of BB modes are bifurcated as one SDB mode and one BB mode. Third, if the number of mistune blades is more than the number of BB modes, then the BB modes do not exist. For example, a single-disk and six-blade rotor system has three asymmetric mistune blades, and all modes are SDB (see Table 3). Fourth, with different tune systems, the error shows a negative deviation in the mistune blade rotor when using ANSYS. Finally, $1c_{11}$ (SDB) modes of the shaft predominates is not affected by mistune blades.

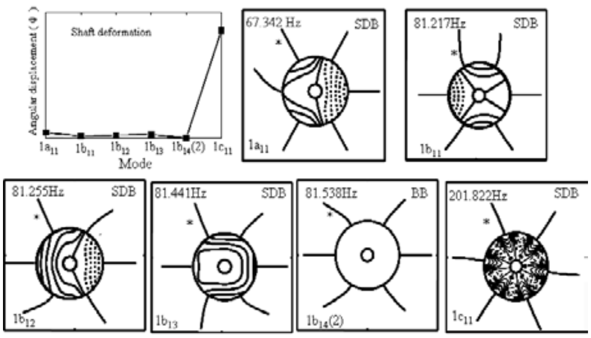

Fig 7. Seven modes of six-blade and single-disk rotor with one blade mistune +10% using AMM.

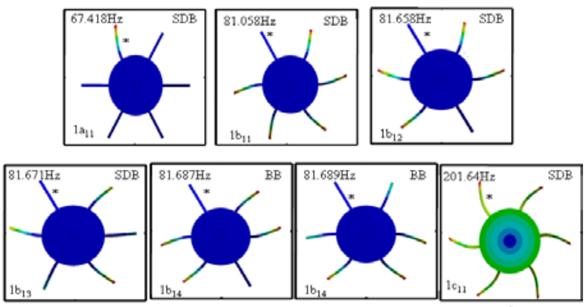

Fig. 8. Seven modes of a six-blade and single-disk rotor with one blade mistune +10% using FEM.

Figures 6-10 show the mode shapes of single flexible disks and six-blade with mistune blades by AMM and ANSYS. The x–y figure shows the shaft torsion displacement. The deflections of the blade and disk are shown in the diagrams. The mode type and NF are indicated at the upper-right and upper-left on each plot. Figs.8 and 10 show the modes by ANSYS, and the others show the modes by AMM. The results from these figures and Tables 3 and 4 show some interesting phenomena. Most notable is that all outcomes match using AMM and ANSYS.

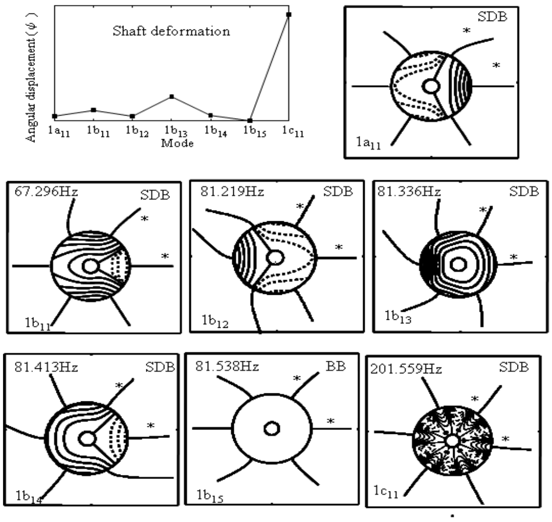

Fig. 9. Seven modes of a six-blade and single-disk rotor with two blades (1,2) mistune +10% using AMM

We understand why the methods are somewhat different (Chiu et al., 2017; Chiu et al., 2017). First, we knew the numbers of frequencies that the blade's first mode leads is Nb and the shaft's first mode predominates $1c_{11}$ are 1 (one). Second, when using the assumed mode method, the rotor is a torsional shaft of fix free, transverse disk of clamp free and bending blade of fix free. From the numerical results, we find that the disk deformation is much smaller than that of the blade and shaft; these are $w_d / v_b \approx 10^{-3} \sim 10^{-4}$ and $w_d / \phi \approx 10^{-3} \sim 10^{-4}$, respectively. Because the NF changes, the disk mode cannot be ignored. Using FEM, the deformation is less than the error of the set, and it can be ignored. So, the modes are right in the assumed mode method. Third, in the $1a_{11}$ and $1c_{11}$ modes, from blade deformation situation; it is convinced that there are SDB modes, although 1a11 mode has no disk deformation in Figs.8 and 10. The $1b_{14}$ modes are repeated modes in these figures. The NF of two modes are close, and the blade deformation is similar; hence, we could say that there are repeated BB modes in Table 3. After comparison, we could say that our results are right. The numbers of mistune blades increase and the disk's deformation becomes more complex. $1c_{11}$ (SDB) modes of the shaft predominate, the blade joined coupled slightly and the disk maintains the invariable symmetric mode. Finally, let us see Figs. 8 and 10. We could not find different situations from the disk between the tune system and mistune blade system. We could say that FEM is not suitable to analyze these complicated change phenomena of coupling vibration in a multi-disc rotor with multi mistune blades.

Table 5. Six modes of NF (Hz) of a five-blade and single flexible disk with disorder angle blades (+30°) using two methods.

Mode	AMM (disorder,1)	FEM (disorder,1)	Deviation (%)	AMM (disorder,1,2)	FEM (disorder,1,2)	Deviation (%)
$1a_{11}$	81.265 (SDB)	80.996 (SDB)	-0.331	81.265 (SDB)	81.085 (SDB)	-0.221
$1b_{11}$	81.449 (SDB)	81.403 (SDB)	-0.056	81.265 (SDB)	81.42 (SDB)	0.191
$1b_{12}$	81.512 (SDB)	81.496 (SDB)	-0.020	81.449 (SDB)	81.516 (SDB)	0.082
$1b_{13}$	81.538 (BB)	81.544 (BB)	0.007	81.512 (SDB)	81.567 (SDB)	0.067
$1b_{13}$	81.538 (BB)	81.621 (BB)	0.102	81.538 (BB)	81.618 (BB)	0.098
$1c_{11}$	202.777 (SDB)	201.93 (SDB)	-0.418	202.777 (SDB)	200.57 (SDB)	-1.088

Table 5 shows the six modes of NFs of a five-blade and single flexible disk with disorder angle blades (+30°) using two methods. The phenomenon of disorder angle blades system has the same situation. But the frequencies change slightly from the system with mistuned blades.

The next case study discussed frequency variation due to symmetric mistune blade in a six-blades and a single disk rotor is displayed in Table 6 and Figure 11. When the mistune blades appear in the symmetric blade, the phenomenon of coupled vibration is interesting and different. First, the modes of predominates by cantilevered first bending of blade display order are; SDB ($1a_{11}$), DB ($1b_{11}$), SDB ($1b_{12}$), DB ($1b_{13}$) and repeat BB ($1b_{14}$) modes in mistune blades locate in numbers 1 and 4 blade of the rotor system. If the mistune blades locate in number 1, 3 and 5, the modes arise order are SDB, DB, SDB, DB and repeat BB ($1b_{14}$) modes bifurcate SDB and BB modes. If the mistune blades locate in number 1, 2, 4, and 5, then the mode sequences are SDB, DB, SDB, DB, SDB, and DB, and the BB mode disappears. Finally, the $1c_{11}$ (SDB) modes of the shaft predominate and are not affected by the mistune blades.

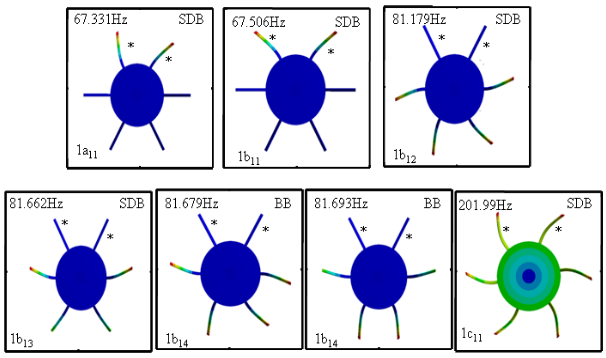

Fig. 10. Seven modes of a six-blade and single-disk rotor with two blades (1,2) mistune +10% using FEM.

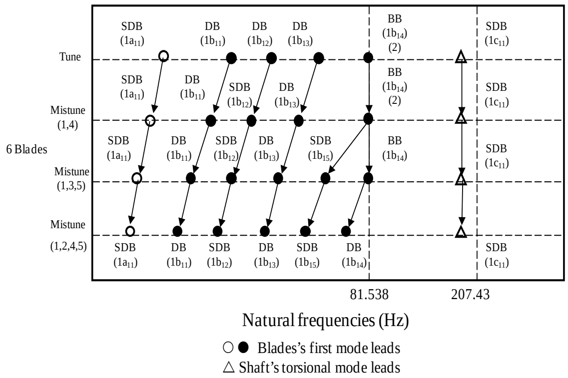

Fig. 11. Frequency variation based on symmetric mistuned blades in a six-blade and single-disk system.

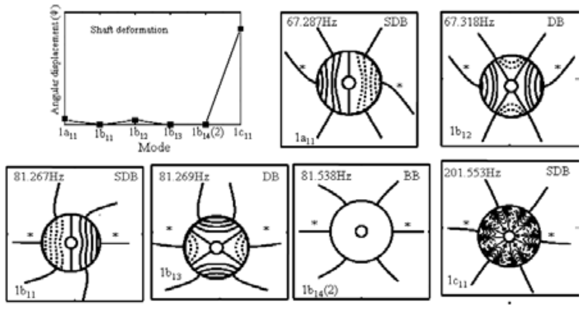

Fig. 12. Seven modes of a six-blade and single-disk rotor with two blades (1,4) mistune +10% using AMM

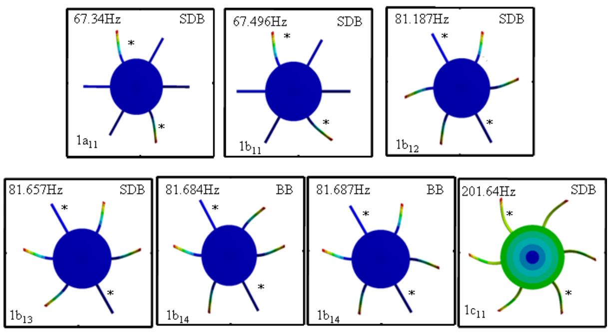

Fig. 13. Seven modes of a six-blade and single-disk rotor with two blades (1,4) mistune +10% using FEM

Figures 12 and 13 show the mode shapes in the case of a six-blade and single flexible disk with symmetric mistune blades by AMM. Although the disk's balance is destroyed because of mistune damage, we find a new equilibrium from the symmetry of mistune, such as $1b_{11}$ and $1b_{13}$ modes. These always are DB modes. $1c_{11}$ (SDB) modes of the shaft predominate, the blade joined coupled slightly, and the disk maintains the symmetric mode. Finally, we compared Figs. 8 and 10, and found that we can hardly distinguish mode shapes or frequencies different from the mistune or tune system using ANSYS. So, FEM is not a good method for these studies.

Table 6. Seven modes of NF (Hz) of a six-blade and single flexible disk with mistune (+10%) blades in the symmetric system using AMM

Mode	AMM (mistune,14)	FEM (mistune,14)	Deviation (%)	AMM (mistune,135)	FEM (mistune,135)	Deviation (%)
$1a_{11}$	67.287 (SDB)	67.34 (SDB)	0.079	67.281 (SDB)	67.262 (SDB)	-0.028
$1b_{11}$	67.318 (DB)	67.496 (DB)	0.264	67.313 (DB)	67.496 (DB)	0.272
$1b_{12}$	81.267 (SDB)	81.187 (SDB)	-0.098	67.394 (DB)	67.496 (SDB)	0.151
$1b_{13}$	81.269 (DB)	81.657 (DB)	0.477	81.238 (SDB)	81.319 (DB)	0.100
$1b_{14}$	81.538 (BB)	81.684 (BB)	0.179	81.327 (DB)	81.671 (SDB)	0.423
$1b_{14}$	81.538 (BB)	81.687 (BB)	0.183	81.538 (BB)	81.672 (DB)	0.164
$1c_{11}$	201.553 (SDB)	201.64 (SDB)	0.043	201.289 (SDB)	201.29 (SDB)	0.0005

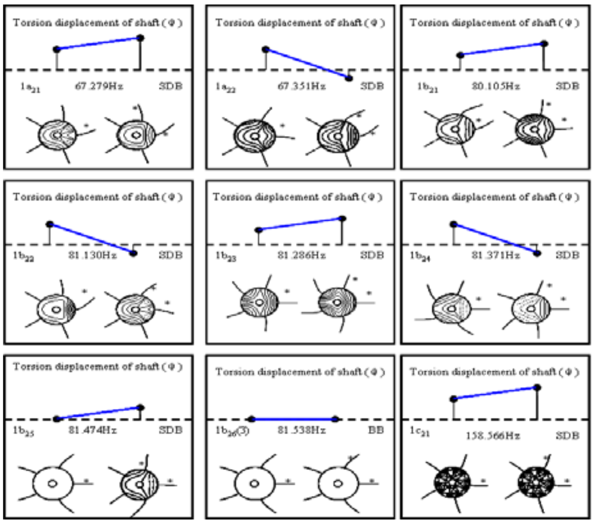

Fig. 14. Night modes of a five-blade and two-disk rotor with three blades (*) mistune and disorder using AMM

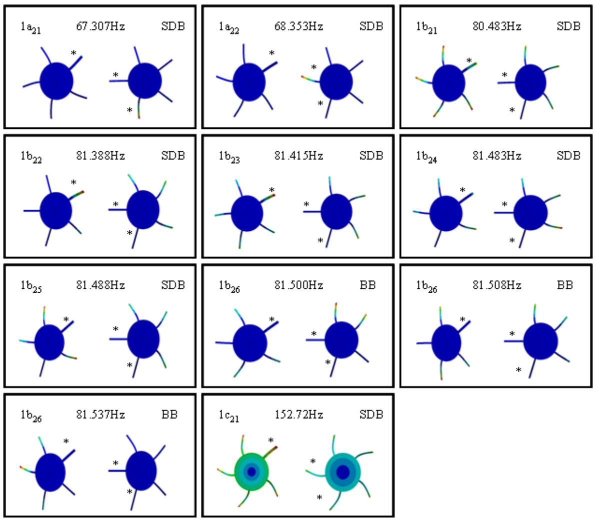

Fig. 15. Night modes of a five-blade and two-disk rotor with three blades (*) mistune and disorder by FEM

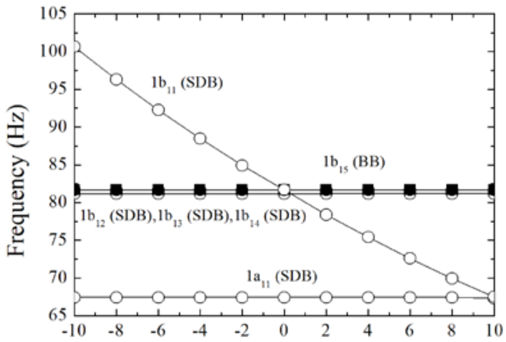

Fig. 16. 1a and1b mode frequency changes with length error of blade for a six-blade rotor

Figures 14 and 15 show the mode shapes of a five-blade and two flexible-disc with three mistune and disorder blades by AMM and ANSYS. The first disk has disorder angle blades (+30°) located in the marked (*) blade, and the second disk has two blades (1,2) mistune +10% in the marked (*) blades. The upper x-y figure shows the shaft torsion displacement. The deflections of blade and disk are illustrated in the diagrams. The mode type and NF are indicated on each plot's middle line. The two cases are compared in Tables 3 and 5, from which it is seen that the system will retain mode shapes and frequencies in a single-disk system and will combine with each other. In other words, they are linear relations. At the same time, we can hardly distinguish mode shapes or frequencies that are different from mistune (disk 2) and disorder (disk 1) systems using ANSYS software.

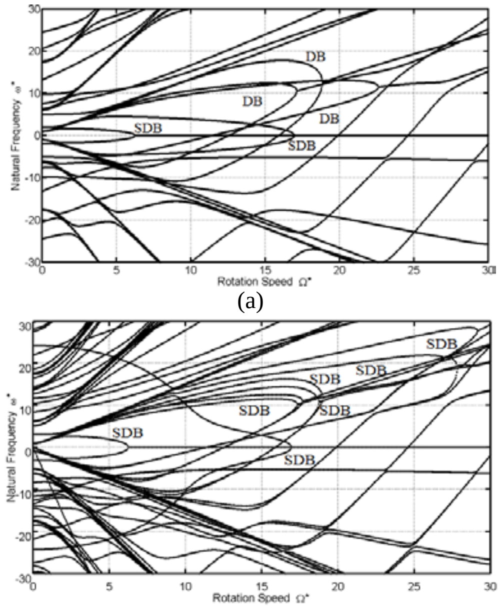

Fig. 17. Variation of eigenvalues with rotation speed for a five-blade in two disk rotors. (a) tune system and (b) two mistuned and a disorder blades system.

We explored how frequencies change with length error of a blade for a six-blade system, as shown in Figure 16. We set blade (1) at 10% mistune, and blade (2) has mistune from -10% to +10%. From Fig.16, we find two results. The frequencies of the $1a_{11}$ and $1b_{12}$ to $1b_{15}$ modes are unchanged in the length error of blade variation. It is seen that the frequencies of $1b_{11}$ (SDB) modes decrease from 100.63 Hz to 67.50 Hz with increasing blade (2) length error. In other words, the mistuned and disorder affect frequency and mode in the multi mistuned blades rotor system, respectively.

In our last case, we describe the rotor's natural frequencies as they vary with rotation. The numerical results are normalized with respect to the first-order natural frequency (ω_{b1}) of the cantilever blade, that is, $\omega^*=\omega/\omega_{b1}$, $\Omega^*=\Omega\ /\omega_{b1}$. Figure 17 explores the two-disk and five-blade rotor system. In Fig.17, the system frequency bifurcates at modes (see Figs. 14 and 15). For forward and backward frequencies close to each other, when the rotation increases, the frequencies merge and ultimately become one. At this merge point, the system has a possible instability. Fig. 17(a) shows a tuned system. Fig. 17(b) shows two mistuned and a disorder blades system. Comparing these two figures, we can find that variation of eigenvalues with rotation speed with a mistuned effect can become complex and unstable.

CONCLUSIONS

Based on previous research, we completely consummated the blade-bending, shaft-torsion and disk-transverse coupled vibration phenomenon of the multi-flexible-disc rotor system. The blade subsystem has mistuned blade lengths or disordered straggle angle blades. We mainly used the AMM and FEM is the complementary one to analyze the system. We compared their results. The research started with the modes change resulting from a five/six blades and flexible disk rotor. The coupling modes could be displayed in three group's types, the SDB, DB and BB. Two of the most interesting things are that symmetry of mistuned blades or disordered straggle angle will cause balance, which get misjudgment of frequency and model. As the numbers of mistuned/disordered blades increase, the disk's deformation become more complex.

After comparing the results of AMM and FEM (using ANSYS), we can confirm our previous research. But the results from ANSYS had some shortcomings. For example, we could not see the disk's deformation, and we could not observe that inter-blade (BB) modes are repeated modes. So, we hardly distinguish mode shapes or frequencies which are different from mistune or disorder by using disk mode shapes. For these reasons, we could say that FEM is only complementary when we analyze these complicated change phenomena of coupled vibration in a multi-disc rotor with multiple mistune or disorder blades.

We found two quantitative results. The frequencies of the $1a_{11}$ and $1b_{12}$ to $1b_{15}$ modes are unchanged in the length error of blade variation. The frequencies of $1b_{11}$ (SDB) modes seem to decrease from 100.63 Hz to 67.50 Hz with increasing blade length error. The rotation effect was also explored, and the authors found that the mistuned effect would become complex and precarious.

ACKNOWLEDGMENT

This work was supported by the Scientific Research Climbing Project of Xiamen University of Technology, No. XPDKT18016.

REFERENCES

Alok S., "Reduced-order model of a bladed rotor with geometric mistuning," *Proceedings of the ASME Turbo Expo*, Vol. 5, pp. 307-314(2007).

Bai B., BAI G.C., LI C., "Application of improved hybrid interface substructural component modal synthesis method in vibration characteristics of mistuned blisk," *Chinese Journal of Mechanical Engineering*, Vol.27, No.6, pp.1219-1231(2014).

Bai B., BAI G.C., LI C., Zhao H.Y., Yao W., "Vibratory characteristic analysis of integral mistuned bladed disk assemblies for aeroengine," *Proc IMechE Part C: J Mechanical Engineering Science*, Vol.229, No.16, pp.2921–2938(2015).

Chen, Y.F., Shen, I.Y., "Mathematical insights into linear mode localization in nearly cyclic symmetric rotors with mistune," *Journal of Vibration and Acoustics, Transactions of the ASME*, Vol.137, No.4, (2015).

Chiu Y.J., Huang S.C., "The influence on coupling vibration of a rotor system due to a mistuned blade length," *International Journal of Mechanical Sciences*, Vol. 49, No. 4, , pp. 522-532(2007).

Chiu Y.J., Huang S.C., "The influence of a mistuned blade's staggle angle on the vibration and stability of a shaft-disk-blade assembly," *Shock and Vibration*, Vol.15, No.1, pp.3-17(2008).

Chiu Y.J., Huang S.C., "The influence of a cracked blade on rotor's free vibration," *ASME, Journal of Vibration and Acoustics*, Vol.130, No.5, 054502(2008).

Chiu Y.J., Jian S.R., Yang C.H., Yu G.F., "Based on lacing wires influence of coupling vibration of a multi flexible disks turbine rotor system by two methods."*Journal of Vibroengineering*, Vol. 19, No. 2, pp.1314-1331(2017).

Chiu, Y.J., Li, X.Y., Chen, Y.C., Jian, S.R., Yang, C.H. and Lin, I.H., "Three methods for studying coupled vibration in a multi flexible disk rotor system," *Journal of Mechanical Science and Technology*, Vol. 31, No. 11, pp. 5219- 5229 (2017).

Gennaro S., Leonardo L., "Non deterministic approaches for the evaluation of the mistune effects on the rotor dynamics," *Collection of Technical Papers -AIAA/ASME/ASCE/AHS/ASC Structures, Structural Dynamics and Materials Conference*, Vol.4, pp.2579-2590(2004).

Hiroki T., Akihiro M., "Vibration characteristics of mistuned bladed disk by sensitivity analysis," *Transactions of the Japan Society of Mechanical Engineers*, Part C, Vol. 78, No. 5, pp. 12-26(2012).

Han D. J., "Complex harmonic modal analysis of rotor systems," *Journal of Mechanical Science and Technology*, Vol.29, No.7, pp. 2735-2746(2015).

Kwon S.M., Yoo H.H., "Vibration localization of a mistuned rotating multi-packet blade system undergoing external cyclic harmonic force," *Journal of Mechanical Science and Technology*, Vol.25, No.11, pp. 2769-2774(2011).

Kwon S.M., Yoo H.H., "Mode and Transient Response Localization Occurred in Rotating Multi-Packet Blade Systems due to Random Mistuning," *International Journal of Precision Engineering and Manufacturing*, Vol.16, No.10, pp.2063-2071(2015).

Li C.F., Zhou S.H., Yang S.H., Ren X., Wen B.C., "Dynamic characteristics of blade-disk-rotor system with structural mistuned features," *Open Mechanical Engineering Journal*, Vol.8, No.1, pp.138-143(2014).

Lee I., Shin S.J., Kim Y.R., "Mistuned bladed disk forced vibration analysis based on standing wave formulation," *Aerospace Science and Technology*, Vol.1, pp.1-8(2011).

Paolo B., Giovanni C., "A continuous model for the dynamical analysis of mistuned bladed rotors," *International Journal of Rotating Machinery*, Vol. 2012, (2012).

Raeisi E., Ziaei-Rad S. "The worst response of mistuned bladed disk system using neural network and genetic algorithm," *Meccanica*, Vol.48, pp.367–379 (2013).

Yasharth B., Alok S., "Reduced order model of a multistage bladed rotor with geometric mistuning via modal analyses of finite element sectors," *Journal of Turbomachinery*, Vol.134, No.4, (2012).

Yu, G.F., Chiu, Y.J., Yang, C.H., Sheng, J. and Li, X.Y., "Exploration of coupled-vibration phenomena in multi-disc rotor with blades with multi-cracks." *Advances in Mechanical Engineering*, Vol. 11, No. (4), pp.1-22(2019)

Zhou S.T., Chiu Y.J., Yu G.F., Yang C.H., Huang H.W., Jian S.R., "An assumed mode method and finite element method investigation of the coupled vibration in a flexible-disk rotor system with lacing wires." *Journal of Mechanical Science and Technology*, Vol.31, No.2, pp.577-586(2017).

APPENDIX

$$[\mathrm{M}]=\begin{bmatrix}
[\mathrm{M}_s]_{(n_s\times n_s)1} & [0]_{(n_s\times n_d)N_d} & [0]_{(n_s\times n_d)N_d} & [\mathrm{M}_{sb}]_{(n_s\times n_b)N_d} & [\mathrm{M}_{sb}]_{(n_s\times n_b)N_d} & \cdots & [\mathrm{M}_{sb}]_{(n_s\times n_b)N_d} \\
[0]^T_{(n_d\times n_s)N_d} & [\mathrm{M}_d^s]_{(n_d\times n_d)N_d} & [0]_{(n_d\times n_d)N_d} & [\mathrm{M}_{db}^s]_{(n_d\times n_b)N_d} & [\mathrm{M}_{db}^s]_{(n_d\times n_b)N_d} & \cdots & [\mathrm{M}_{db}^s]_{(n_d\times n_b)N_d} \\
[0]^T_{(n_d\times n_s)N_d} & [0]_{(n_d\times n_d)N_d} & [\mathrm{M}_d^c]_{(n_d\times n_d)N_d} & [\mathrm{M}_{db}^{*c}]_{(n_d\times n_b)N_d} & [\mathrm{M}_{db}^c]_{(n_d\times n_b)N_d} & \cdots & [\mathrm{M}_{db}^c]_{(n_d\times n_b)N_d} \\
[\mathrm{M}_{sb}^*]^T_{(n_b\times n_s)N_d} & [\mathrm{M}_{db}^{*s}]^T_{(n_b\times n_d)N_d} & [\mathrm{M}_{db}^{*c}]^T_{(n_b\times n_d)N_d} & [\mathrm{M}_b^*]_{(n_b\times n_b)N_d} & [0]_{(n_b\times n_b)N_d} & \cdots & [0]_{(n_b\times n_b)N_d} \\
[\mathrm{M}_{sb}]^T_{(n_b\times n_s)N_d} & [\mathrm{M}_{db}^s]^T_{(n_b\times n_d)N_d} & [\mathrm{M}_{db}^c]^T_{(n_b\times n_d)N_d} & [0]^T_{(n_b\times n_b)N_d} & [\mathrm{M}_b]_{(n_b\times n_b)N_d} & \ddots & \vdots \\
\vdots & \vdots & \vdots & \vdots & \ddots & \ddots & [0]_{(n_b\times n_b)N_d} \\
[\mathrm{M}_{sb}]^T_{(n_b\times n_s)N_d} & [\mathrm{M}_{db}^s]^T_{(n_b\times n_d)N_d} & [\mathrm{M}_{db}^c]^T_{(n_b\times n_d)N_d} & [0]^T_{(n_b\times n_b)N_d} & \cdots & [0]^T_{(n_b\times n_b)N_d} & [\mathrm{M}_b]_{(n_b\times n_b)N_d}
\end{bmatrix} \tag{A.1}$$

$$[\mathrm{P}]=\begin{bmatrix}
[0]_{(n_s\times n_s)1} & [0]_{(n_s\times n_d)N_d} & [0]_{(n_s\times n_d)N_d} & [0]_{(n_s\times n_b)N_d} & \cdots & \cdots & [0]_{(n_s\times n_b)N_d} \\
[0]^T_{(n_d\times n_s)N_d} & [\mathrm{P}_d^s]_{(n_d\times n_d)N_d} & [0]_{(n_d\times n_d)N_d} & [0]_{(n_d\times n_b)N_d} & \cdots & \cdots & [0]_{(n_d\times n_b)N_d} \\
[0]^T_{(n_d\times n_s)N_d} & [0]_{(n_d\times n_d)N_d} & [\mathrm{P}_d^c]_{(n_d\times n_d)N_d} & [0]_{(n_d\times n_b)N_d} & \cdots & \cdots & [0]_{(n_d\times n_b)N_d} \\
[0]^T_{(n_b\times n_s)N_d} & [0]^T_{(n_b\times n_d)N_d} & [0]^T_{(n_b\times n_d)N_d} & [0]_{(n_b\times n_b)N_d} & [0]_{(n_b\times n_b)N_d} & \cdots & [0]_{(n_b\times n_b)N_d} \\
[0]^T_{(n_b\times n_s)N_d} & [0]^T_{(n_b\times n_d)N_d} & [0]^T_{(n_b\times n_d)N_d} & [0]^T_{(n_b\times n_b)N_d} & \ddots & \ddots & \vdots \\
\vdots & \vdots & \vdots & \vdots & \ddots & \ddots & [0]_{(n_b\times n_b)N_d} \\
[0]^T_{(n_b\times n_s)N_d} & [0]^T_{(n_b\times n_d)N_d} & [0]^T_{(n_b\times n_d)N_d} & [0]^T_{(n_b\times n_b)N_d} & \cdots & [0]^T_{(n_b\times n_b)N_d} & [0]_{(n_b\times n_b)N_d}
\end{bmatrix} \tag{A.2}$$

$$[\mathrm{K}^e]=\begin{bmatrix}
[\mathrm{K}_s^e]_{(n_s\times n_s)1} & [0]_{(n_s\times n_d)N_d} & [0]_{(n_s\times n_d)N_d} & [0]_{(n_s\times n_b)N_d} & \cdots & \cdots & [0]_{(n_s\times n_b)N_d} \\
[0]^T_{(n_d\times n_s)N_d} & [\mathrm{K}_d^{es}]_{(n_d\times n_d)N_d} & [0]_{(n_d\times n_d)N_d} & [0]_{(n_d\times n_b)N_d} & \cdots & \cdots & [0]_{(n_d\times n_b)N_d} \\
[0]^T_{(n_d\times n_s)N_d} & [0]_{(n_d\times n_d)N_d} & [\mathrm{K}_d^{ec}]_{(n_d\times n_d)N_d} & [0]_{(n_d\times n_b)N_d} & \cdots & \cdots & [0]_{(n_d\times n_b)N_d} \\
[0]^T_{(n_b\times n_s)N_d} & [0]^T_{(n_b\times n_d)N_d} & [0]^T_{(n_b\times n_d)N_d} & [\mathrm{K}_b^e]_{(n_b\times n_b)N_d} & [0]_{(n_b\times n_b)N_d} & \cdots & [0]_{(n_b\times n_b)N_d} \\
[0]^T_{(n_b\times n_s)N_d} & [0]^T_{(n_b\times n_d)N_d} & [0]^T_{(n_b\times n_d)N_d} & [0]^T_{(n_b\times n_b)N_d} & \ddots & \ddots & \vdots \\
\vdots & \vdots & \vdots & \vdots & \ddots & \ddots & [0]_{(n_b\times n_b)N_d} \\
[0]^T_{(n_b\times n_s)N_d} & [0]^T_{(n_b\times n_d)N_d} & [0]^T_{(n_b\times n_d)N_d} & [0]^T_{(n_b\times n_b)N_d} & \cdots & [0]^T_{(n_b\times n_b)N_d} & [\mathrm{K}_b^e]_{(n_b\times n_b)N_d}
\end{bmatrix} \tag{A.3}$$

$$[\mathrm{K}^\Omega]=\begin{bmatrix}
[\mathrm{K}_s^\Omega]_{(n_s\times n_s)1} & [0]_{(n_s\times n_d)N_d} & [0]_{(n_s\times n_d)N_d} & [\mathrm{K}_{sb}^\Omega]_{(n_s\times n_b)N_d} & \cdots & \cdots & [\mathrm{K}_{sb}^\Omega]_{(n_s\times n_b)N_d} \\
[0]^T_{(n_d\times n_s)N_d} & [\mathrm{K}_d^{\Omega s}]_{(n_d\times n_d)N_d} & [0]_{(n_d\times n_d)N_d} & [0]_{(n_d\times n_b)N_d} & \cdots & \cdots & [0]_{(n_d\times n_b)N_d} \\
[0]^T_{(n_d\times n_s)N_d} & [0]_{(n_d\times n_d)N_d} & [\mathrm{K}_d^{\Omega c}]_{(n_d\times n_d)N_d} & [0]_{(n_d\times n_b)N_d} & \cdots & \cdots & [0]_{(n_d\times n_b)N_d} \\
[\mathrm{K}_{sb}^\Omega]^T_{(n_b\times n_s)N_d} & [0]^T_{(n_b\times n_d)N_d} & [0]^T_{(n_b\times n_d)N_d} & [\mathrm{K}_b^\Omega]_{(n_b\times n_b)N_d} & [0]_{(n_b\times n_b)N_d} & \cdots & [0]_{(n_b\times n_b)N_d} \\
[\mathrm{K}_{sb}^\Omega]^T_{(n_b\times n_s)N_d} & [0]^T_{(n_b\times n_d)N_d} & [0]^T_{(n_b\times n_d)N_d} & [0]^T_{(n_b\times n_b)N_d} & \ddots & \ddots & \vdots \\
\vdots & \vdots & \vdots & \vdots & \ddots & \ddots & [0]_{(n_b\times n_b)N_d} \\
[\mathrm{K}_{sb}^\Omega]^T_{(n_b\times n_s)N_d} & [0]^T_{(n_b\times n_d)N_d} & [0]^T_{(n_b\times n_d)N_d} & [0]^T_{(n_b\times n_b)N_d} & \cdots & [0]^T_{(n_b\times n_b)N_d} & [\mathrm{K}_b^\Omega]_{(n_b\times n_b)N_d}
\end{bmatrix} \tag{A.4}$$

$$[\mathrm{K}^i]=\begin{bmatrix}
[0]_{(n_s\times n_s)1} & [0]_{(n_s\times n_d)N_d} & [0]_{(n_s\times n_d)N_d} & [0]_{(n_s\times n_b)N_d} & \cdots & \cdots & [0]_{(n_s\times n_b)N_d} \\
[0]^T_{(n_d\times n_s)N_d} & [\mathrm{K}_d^{is}]_{(n_d\times n_d)N_d} & [0]_{(n_d\times n_d)N_d} & [0]_{(n_d\times n_b)N_d} & \cdots & \cdots & [0]_{(n_d\times n_b)N_d} \\
[0]^T_{(n_d\times n_s)N_d} & [0]_{(n_d\times n_d)N_d} & [\mathrm{K}_d^{ic}]_{(n_d\times n_d)N_d} & [0]_{(n_d\times n_b)N_d} & \cdots & \cdots & [0]_{(n_d\times n_b)N_d} \\
[0]^T_{(n_b\times n_s)N_d} & [0]^T_{(n_b\times n_d)N_d} & [0]^T_{(n_b\times n_d)N_d} & [0]_{(n_b\times n_b)N_d} & [0]_{(n_b\times n_b)N_d} & \cdots & [0]_{(n_b\times n_b)N_d} \\
[0]^T_{(n_b\times n_s)N_d} & [0]^T_{(n_b\times n_d)N_d} & [0]^T_{(n_b\times n_d)N_d} & [0]^T_{(n_b\times n_b)N_d} & \ddots & \ddots & \vdots \\
\vdots & \vdots & \vdots & \vdots & \ddots & \ddots & [0]_{(n_b\times n_b)N_d} \\
[0]^T_{(n_b\times n_s)N_d} & [0]^T_{(n_b\times n_d)N_d} & [0]^T_{(n_b\times n_d)N_d} & [0]^T_{(n_b\times n_b)N_d} & \cdots & [0]^T_{(n_b\times n_b)N_d} & [0]^T_{(n_b\times n_b)N_d}
\end{bmatrix} \tag{A.5}$$

$$[\mathrm{M}_s]_{ij}=\int_0^{Ls} I_s\Phi_i\Phi_j dZ+I_d[\Phi_i\Phi_j]_{Z=Z_d}+\rho_b A_b\sum_1^{N_b}\int_{r_d}^{r_b}x^2[\Phi_i\Phi_j]_{Z=Z_d}\,dx \tag{A.6}$$

$$[\mathrm{M}_{sb}]_{ij}=\rho_b A_b\int_{r_d}^{r_b}x\Phi_i|_{Z=Z_d}V_j\cos\beta_k\,dx \tag{A.7}$$

$$[\mathrm{M}_b]_{ij}=\rho_b A_b\int_{r_d}^{r_b}V_iV_j\,dx \tag{A.8}$$

$$
\begin{aligned}
[\mathrm{M}_d]_{ij} &= \rho_d h_d \left\{ \int_{r_s}^{r_d}\int_0^{2\pi} W_i^s W_j^s r d\theta dr + \int_{r_s}^{r_d}\int_0^{2\pi} W_i^c W_j^c r d\theta dr \right\} \\
&+ \rho_b A_b \sum_1^{N_b} \int_{r_d}^{r_b} \left\{ [W_i^s W_j^s]_{\substack{r=r_d\\ \theta=\bar\theta}} + x_k [W_i^s \left(\frac{\partial W_j^s}{\partial r}\right) + \left(\frac{\partial W_i^s}{\partial r}\right) W_j^s]_{\substack{r=r_d\\ \theta=\bar\theta}} \right. \\
&\left. + x^2 [\left(\frac{\partial W_i^s}{\partial r}\right)\left(\frac{\partial W_j^s}{\partial r}\right)]_{\substack{r=r_d\\ \theta=\bar\theta}} \right\} dx \\
&+ \rho_b A_b \sum_1^{N_b} \int_{r_d}^{r_b} \left\{ [W_i^c W_j^c]_{\substack{r=r_d\\ \theta=\bar\theta}} + x_k [W_i^c \left(\frac{\partial W_j^c}{\partial r}\right) + \left(\frac{\partial W_i^c}{\partial r}\right) W_j^c]_{\substack{r=r_d\\ \theta=\bar\theta}} \right. \\
&\left. + x^2 [\left(\frac{\partial W_i^c}{\partial r}\right)\left(\frac{\partial W_j^c}{\partial r}\right)]_{\substack{r=r_d\\ \theta=\bar\theta}} \right\} dx
\end{aligned} \tag{A.9}
$$

$$
\begin{aligned}
[\mathrm{M}_{db}]_{ij} &= -\rho_b A_b \left\{ \int_{r_d}^{r_b} [W_i^s + x\left(\frac{\partial W_i^s}{\partial r}\right)]_{\substack{r=r_d\\ \theta=\bar\theta}} V_j \sin\beta_k dx \right. \\
&\left. + \int_{r_d}^{r_b} [W_i^c + x\left(\frac{\partial W_i^c}{\partial r}\right)]_{\substack{r=r_d\\ \theta=\bar\theta}} V_j \sin\beta_k dx \right\}
\end{aligned} \tag{A.10}
$$

$$
\begin{aligned}
[\mathrm{P}_d^s]_{ij} &= \rho_d h_d \left\{ \int_{r_s}^{r_d}\int_0^{2\pi} [W_i^s \left(\frac{\partial W_j^s}{\partial \theta}\right) + \left(\frac{\partial W_i^s}{\partial \theta}\right) W_j^s] r d\theta dr \right. \\
&\left. + \int_{r_s}^{r_d}\int_0^{2\pi} [W_i^c \left(\frac{\partial W_j^c}{\partial \theta}\right) + \left(\frac{\partial W_i^c}{\partial \theta}\right) W_j^c] r d\theta dr \right\}
\end{aligned} \tag{A.11}
$$

$$
[\mathrm{K}_s^e]_{ij} = \int_0^{Ls} G_s J_s \Phi_i' \Phi_j' dZ \tag{A.12}
$$

$$
\begin{aligned}
[\mathrm{K}_d^e]_{ij} &= D\left\{ \int_{r_s}^{r_d}\int_0^{2\pi} r(\nabla^2 W_i^s)(\nabla^2 W_j^s) dr d\theta + \int_{r_s}^{r_d}\int_0^{2\pi} r(\nabla^2 W_i^c)(\nabla^2 W_j^c) dr d\theta \right\} \\
&+ 2(1-\nu)D\left\{ \int_{r_s}^{r_d}\int_0^{2\pi} \frac{1}{r}[(\frac{\partial^2 W_i^s}{\partial r\partial\theta} - \frac{1}{r}\frac{\partial W_i^s}{\partial\theta})(\frac{\partial^2 W_j^s}{\partial r\partial\theta} - \frac{1}{r}\frac{\partial W_j^s}{\partial\theta})] d\theta dr \right. \\
&\left. + \int_{r_s}^{r_d}\int_0^{2\pi} \frac{1}{r}[(\frac{\partial^2 W_i^c}{\partial r\partial\theta} - \frac{1}{r}\frac{\partial W_i^c}{\partial\theta})(\frac{\partial^2 W_j^c}{\partial r\partial\theta} - \frac{1}{r}\frac{\partial W_j^c}{\partial\theta})] d\theta dr \right\} \\
&- (1-\nu)D\left\{ \int_{r_s}^{r_d}\int_0^{2\pi} \left[(\frac{\partial^2 W_i^s}{\partial r^2})(\frac{\partial W_j^s}{\partial r} + \frac{1}{r}\frac{\partial^2 W_j^s}{\partial\theta^2}) + (\frac{\partial W_i^s}{\partial r} + \frac{1}{r}\frac{\partial^2 W_i^s}{\partial\theta^2})(\frac{\partial^2 W_j^s}{\partial r^2}) \right] d\theta dr \right. \\
&\left. + \int_{r_s}^{r_d}\int_0^{2\pi} \left[(\frac{\partial^2 W_i^c}{\partial r^2})(\frac{\partial W_j^c}{\partial r} + \frac{1}{r}\frac{\partial^2 W_j^c}{\partial\theta^2}) + (\frac{\partial W_i^c}{\partial r} + \frac{1}{r}\frac{\partial^2 W_i^c}{\partial\theta^2})(\frac{\partial^2 W_j^c}{\partial r^2}) \right] d\theta dr \right\}
\end{aligned} \tag{A.13}
$$

$$
[\mathrm{K}_b^e]_{ij} = E_b I_A \int_{r_d}^{r_b} V_i'' V_j'' dx \tag{A.14}
$$

$$
\begin{aligned}
[\mathrm{K}_d^i]_{ij} &= h_d \left\{ \int_{r_s}^{r_d}\int_0^{2\pi} [\sigma_r \left(\frac{\partial W_i^s}{\partial r}\right)\left(\frac{\partial W_j^s}{\partial r}\right) + \frac{\sigma_\theta}{r^2}\left(\frac{\partial W_i^s}{\partial \theta}\right)\left(\frac{\partial W_j^s}{\partial \theta}\right)] d\theta dr \right. \\
&\left. + \int_{r_s}^{r_d}\int_0^{2\pi} [\sigma_r \left(\frac{\partial W_i^c}{\partial r}\right)\left(\frac{\partial W_j^c}{\partial r}\right) + \frac{\sigma_\theta}{r^2}\left(\frac{\partial W_i^c}{\partial \theta}\right)\left(\frac{\partial W_j^c}{\partial \theta}\right)] d\theta dr \right\}
\end{aligned} \tag{A.15}
$$

$$
[\mathrm{K}_s^\Omega]_{ij} = \frac{1}{2}\rho_b A_b \sum_1^{N_b} \int_{r_d}^{r_b} (r_b^2 - 3x^2)[\Phi_i \Phi_j]_{Z=Z_d} dx \tag{A.16}
$$

$$
[\mathrm{K}_{sb}^\Omega]_{ij} = \rho_b A_b \int_{r_d}^{r_b} x\Phi_i\Big|_{Z=Z_d} V_j \cos\beta_k dx - \frac{1}{2}\rho_b A_b \int_{r_d}^{r_b} (r_b^2 - x^2)\Phi_i\Big|_{Z=Z_d} V_j' \cos\beta_k dx \tag{A.17}
$$

$$
[\mathrm{K}_d^\Omega]_{ij} = \rho_d h_d \left\{ \begin{aligned} &\int_{r_s}^{r_d}\int_0^{2\pi} \left(\frac{\partial W_i^s}{\partial \theta}\right)\left(\frac{\partial W_j^s}{\partial \theta}\right) r d\theta dr \\ &+ \int_{r_s}^{r_d}\int_0^{2\pi} \left(\frac{\partial W_i^c}{\partial \theta}\right)\left(\frac{\partial W_j^c}{\partial \theta}\right) r d\theta dr \end{aligned} \right\} \tag{A.18}
$$

$$
[\mathrm{K}_b^\Omega]_{ij} = \rho_b A_b \int_{r_d}^{r_b} V_i V_j \cos^2\beta_k dx - \frac{1}{2}\rho_b A_b \int_{r_d}^{r_b} \left(r_b^2 - x^2\right) V_i' V_j' dx \tag{A.19}
$$

NOMENCLATURE

q	generalized vector
v_b	blade displacement with respect to the Y_2 axis
$\hat{v}_b$	blade displacement with respect to the Y_3 axis
N_b	Blades' numbers
V_i	bending blade's mode shapes
ϕ	shaft-disk torsional displacement relative to rotation frame
ω	nature frequency
ω^*	dimensionless nature frequency ($\omega^* = \omega / \omega_{b1}$)
τ_i	beam function's frequency with fixed-free end
Ω	rotational speed
Ω^*	dimensionless rotational speed ($\Omega^* = \Omega / \omega_{b1}$)

Subscripts

$(\ )_s$	shaft
$(\ )_d$	disk
$(\ )_b$	blade

葉片長度失調及攻角角度失序的多盤轉子耦合振動線性和非線性現象研究

邱亦睿　趙亞正　李曉雲　楊嘉豪
于國飛　葉誠偉
廈門理工學院機械與汽車工程學院

摘 要

本文採用了有限元法和假設模態法，研究具有多個失諧或失序葉片的多圓盤系統的圓盤橫向、葉片彎曲和軸扭轉耦合振動現象。本文對轉子系統固有頻率和振型的變化規律進行了研究和比較。數值計算結果表明，失諧或失序葉片的數量以及對稱性都會影響葉片的固有頻率。在定量分析中，作者將葉片(1)設置為 10%的失諧，葉片(2)的失諧範圍為-10%到+10%。當葉片(2)長度有誤差時，$1a_{11}$ 和 $1b_{12}$ 至 $1b_{15}$ 模態的頻率是保持不變的。葉片(2)長度誤差從-10%增加到 10%，$1b_{11}$(SDB)模態的頻率從 100.63Hz 下降到 67.50 Hz。最後，本文還探討了旋轉效應，發現失諧效應會變得複雜和不穩定。